

## VIV simulation of riser-conductor systems including nonlinear soil-structure interactions

Maokun Ye<sup>\*1</sup> and Hamn-Ching Chen<sup>2a</sup>

<sup>1</sup>Department of Ocean Engineering, Texas A&M University, USA

<sup>2</sup>Zachry Department of Civil Engineering and Department of Ocean Engineering,  
Texas A&M University, USA

(Received February 2, 2019, Revised April 9, 2019, Accepted June 13, 2019)

**Abstract.** This paper presents a fully three-dimensional numerical approach for analyzing deepwater drilling riser-conductor system vortex-induced vibrations (VIV) including nonlinear soil-structure interactions (SSI). The drilling riser-conductor system is modeled as a tensioned beam with linearly distributed tension and is solved by a fully implicit discretization scheme. The fluid field around the riser-conductor system is obtained by Finite-Analytic Navier-Stokes (FANS) code, which numerically solves the unsteady Navier-Stokes equations. The SSI is considered by modeling the lateral soil resistance force according to nonlinear p-y curves. Overset grid method is adopted to mesh the fluid domain. A partitioned fluid-structure interaction (FSI) method is achieved by communication between the fluid solver and riser motion solver. A riser-conductor system VIV simulation without SSI is firstly presented and served as a benchmark case for the subsequent simulations. Two SSI models based on a nonlinear p-y curve are then applied to the VIV simulations. Also, the effects of two key soil properties on the VIV simulations of riser-conductor systems are studied.

**Keywords:** CFD simulation; vortex induced vibrations; fluid-structure interaction; nonlinear soil-structure interaction; riser-conductor system

---

### 1. Introduction

Offshore oil production has experienced a continual increase globally during the last few decades. In the offshore oil production industry, the production conductors are widely used. They are used for offshore wells and served as a foundation for the wellhead. The production conductors are surrounded by seabed soil and connected to floating platforms through a top-tensioned riser and are exposed to complicated environmental forces.

On one hand, the system experiences vortex-induced vibrations (VIV) in ocean water current. VIV has been studied by many researchers and has been an active research area in Ocean Engineering for several years, and both experimental studies and numerical simulations have been applied to this research area. Wilde and Huijsmans (2004) conducted a laboratory experiment at

---

\*Corresponding author, Ph.D. Student, E-mail: leafsunny@tamu.edu

<sup>a</sup> A.P. & Florence Wiley Professor, E-mail: hcchen@civil.tamu.edu

Maritime Research Institute Netherlands (MARIN) in which a steel pipe with a circular cross-section was studied. Riser VIV behavior from several towing speeds (0.5 to 3.0 m/s) and pretensions (0.5 to 2.5 kN) were recorded. Trim *et al.* (2005) conducted a test in Marintek's Ocean Basin of a riser model with a length-to-diameter ratio equal to 1400, in an effort to more accurately predict the fatigue life of risers. Full-scale riser VIV responses with and without VIV suppression are measured in the Gulf of Mexico and reported by Tognarelli *et al.* (2008), and the data is compared with the results calculated by SHEAR7. With the development of computer capability and computational methods, numerical simulations to study pipeline VIV are widely used. Simulations of VIV response for fixed cylinders were conducted by Pontaza *et al.* (2004), using a computational fluid dynamics (CFD) method in conjunction with overset grid technique. Studies on long risers with a length-to-diameter ratio of 1400 were carried out by Huang *et al.* (2007). A tensioned beam motion solver with only in-line and cross-flow displacement was proposed and validated. This approach of VIV simulation was then used to study riser VIV in uniform (Huang *et al.* 2010) and sheared current (Huang *et al.* 2012). The same method was further applied to the simulations of VIV and wake-induced vibration (WIV) of dual risers by Chen *et al.* (2013). Riser fatigue analysis in uniform and shear current was performed by Kamble and Chen (2016), and the result matches the experimental data well. CFD simulations of free-standing hybrid risers are then conducted by Cao and Chen (2017), in which prescribed motion at the top of the riser is used to simulate the motion of the buoyancy can. A beam finite element coupled with a viscous flow solver was used to simulate the VIV of pipes by Pontaza and Menon (2009), and a good agreement with previous research and experiment were reported. The same CFD approach is also used to study the VIV of free span pipelines by combining a linear soil model by Xiao and Chen (2015). A more complex soil model is then used in the VIV simulations of free span pipelines by Zhu (2017).

On the other hand, offshore drilling conductors penetrate into the seabed, thus soil resistance force will be applied to the riser-conductor systems. It is, therefore, necessary to include the soil-structure interactions (SSI) in riser-conductor system VIV simulations. Offshore riser-conductor systems with SSI can be modeled as so-called 'laterally loaded piles' in the soil. In the past several decades, many researchers have studied the behavior of 'laterally loaded piles' in soil, and several well-known SSI analysis methods were proposed. These included Beam on Winkler Foundation method (Nogami *et al.* 1988, 1991, Gazetas and Dobry 1984, Naggar and Novak 1995) continuous medium model method (Basu and Salgado 2007, Han *et al.* 2015), and experimental method (Reese 1974). In particular, the simple and computationally efficient Beam on Winkler Foundation method has been widely used in numerical simulations of pile-soil interactions, since that it conveniently treats continual soil resistance force as discretized equivalent soil springs. Novak *et al.* (1974) modeled the soil resistance force as a series of frequency dependent springs and dashpots. An approximate analytical approach based on linear elasticity is introduced in their work. A more complicated method to model the soil resistance as near field and far field springs is presented by Nogami *et al.* (1988) to analyze pile steady-state harmonic. Nogami *et al.* (1991) further elaborated the previous method to model the near-field soil as frequency dependent springs and dashpots in order to account for soil nonlinear behavior such as slippage and gapping. A different near-field and far-field soil model was also published by EI Naggar and Novak (1995).

In this paper, SSI is achieved by utilizing the p-y method (Matlock 1970) developed based on Beam on Winkler Foundation, which is a numerical approach to simulate the soil-structure interactions as predefined p-y curves, where p is the soil resistance (pressure per unit length of the pile) and y is the pile deflection. The soil is represented by a series of linear or nonlinear p-y

curves which vary with depth and soil properties. This method has been applied to many real world problems since published, and a good ability to simulate static as well as dynamic SSI problems has been reported by previous researchers. An approach combining p-y method and the Newmark method was introduced by Yao *et al.* (2011) to simulate the nonlinear behavior of super-long piles. The results were compared with those obtained by commercial Finite Element Analysis (FEA) software ABAQUS, and a good general agreement was shown. Liang *et al.* (2014) modified the commonly used p-y curves published by Matlock (1970) to evaluate the relatively small soil resistance force near the mudline, and a vehicle-bridge coupled model with nonlinear lateral SSI was analyzed to determine the dynamic responses of the bridge under vehicle loads. The p-y curve method has also been applied to ocean environment with a particular focus on horizontal subsea pipelines. A relatively simple nonlinear p-y curve to model the interaction between seabed soil and the embedded pipe was introduced by Ai and Sun (2010) to simulate the VIV responses of a free span pipeline. Zhu (2017) used a complex nonlinear p-y curve to model the seabed soil-pipe interactions when simulating the VIV responses of free span pipelines. Good agreement with results from previous studies was found.

This paper presents a three-dimensional numerical method of simulating offshore riser-conductor system VIV response. The riser-conductor system is treated as a top-tensioned beam. The soil-structure interactions below the mudline between the conductor and surrounding soil are modeled by certain p-y curves. A fully implicit discretization scheme is applied to solve the partial differential equations which govern the pipe motion. The fluid domain above the mudline is solved numerically by the Finite-Analytic Navier-Stokes (FANS) method of Chen, Patel and Ju (1990).

## 2. Numerical methods

### 2.1 Computational fluid dynamics background

In this paper, the Finite-Analytic Navier-Stokes method of Chen *et al.* (1990) and Pontaza *et al.* (2005) is employed to solve the unsteady incompressible Navier-Stokes equations. Large eddy simulation (LES) with Smagorinsky subgrid-scale model is adopted to calculate the turbulent flow field surrounding the riser-conductor system.

### 2.2 Soil-Structure Interaction (SSI) Models

The SSI models adopted in this paper are based on the method of Beam on Winkler Foundation (Matlock and Reese 1960, Gazetas and Dobry 1984). Lateral soil resistance force along the conductor is discretized to equivalent soil springs which characterized by p-y curves. The p-y curves are based on the p-y curve for soft clay suggested by Matlock (1970), which is also adopted by API Recommended Practice 2GEO for the measure of soil reaction for laterally-load piles. It is worth mentioning that the “y” used in the equations which describe the SSI models represents the pipe lateral displacements, “y” and “z” displacements in the y-z plane. And the “x” used in the equations represents the pipe axial direction.

According to Matlock, the following ultimate resistance per unit length of pipe is recommended

$$p_u = \left( 3c + \gamma x + J \frac{cx}{d} \right) d \quad \text{for } 0 \leq x \leq x_r, \tag{1}$$

$$p_u = 9cd \quad \text{for } x \geq x_r. \tag{2}$$

Where  $p_u$  is soil lateral ultimate resistance per unit length of pipe;  $c$  is the shear strength for soft clay;  $d$  is the diameter of pipe;  $\gamma$  is the effective unit weight of soft clay;  $J$  is a dimensionless empirical constant with values from 0.25 to 0.5, and value of 0.5 is suggested for Gulf of Mexico clays;  $x$  represents the depth below soil surface; and  $x_r$  is the depth of reduced resistance, given as

$$x_r = \frac{6d}{\frac{\gamma d}{c} + J} \tag{3}$$

The proposed load-deflection ( $p$ - $y$ ) curves for soft clay is shown in Fig. 1. The ordinate is normalized by  $p_u$ , and the abscissa is normalized by  $y_c$ , which is given by

$$y_c = 2.5\varepsilon_c d \tag{4}$$

where  $\varepsilon_c$  is the strain which occurs at one-half of the maximum stress on laboratory sample test. A value of 0.010 is suggested by Matlock (1970) for most purposes. When the deflection of the pipe is less than three times of  $y_c$ , that is to say  $y/y_c \leq 3$ , the  $p$ - $y$  curve is described as

$$\frac{p}{p_u} = 0.5 \left( \frac{y}{y_c} \right)^{\frac{1}{3}} \tag{5}$$

For soil at the free surface, which is  $x = 0$ , complete loss of soil resistance is assumed when  $y/y_c \geq 15$ . For soil in the range from free soil surface and depth of reduced resistance, which is  $0 \leq x \leq x_r$ , a constant value of resistance force is given for  $y/y_c \geq 15$

$$\frac{p}{p_u} = 0.72 \left( \frac{x}{x_r} \right) \tag{6}$$

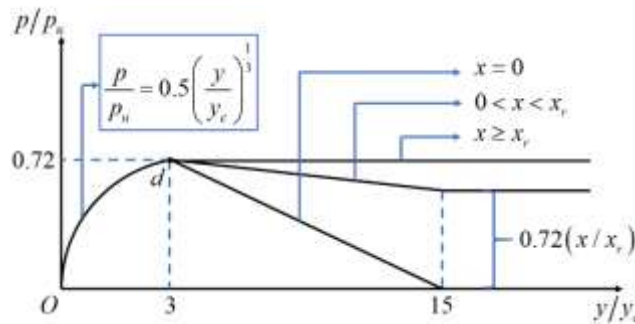


Fig. 1  $p$ - $y$  curves for soft clay

For soil below the depth of reduced resistance,  $x \geq x_r$ , maximum soil resistance of  $0.72 p_u$  is reached at  $y/y_c = 3$ . One simplified p-y curve based on the fully nonlinear p-y curve is presented and used for VIV simulation first. The simplification is made only for the relation between  $p/p_u$  and  $y/y_c$ , as given by Eq. (7)

$$\frac{p}{p_u} = 0.24 \left( \frac{y}{y_c} \right) \tag{7}$$

### 2.3 Pipe motion solver

The riser-conductor system can be simplified as a top tensioned beam with in-line and cross-stream motions. The partial differential equations which govern its lateral motion are as follows

$$T \frac{d^2 y}{dx^2} + \frac{dy}{dx} \frac{dT}{dx} - \frac{d^2}{dx^2} \left( EI \frac{d^2 y}{dx^2} \right) + f_y = m\ddot{y} + D_s \dot{y} \tag{8}$$

$$T \frac{d^2 z}{dx^2} + \frac{dz}{dx} \frac{dT}{dx} - \frac{d^2}{dx^2} \left( EI \frac{d^2 z}{dx^2} \right) + f_z = m\ddot{z} + D_s \dot{z} \tag{9}$$

The  $x$  in the above equations represents the pipe axial direction, which is vertical to the ground;  $y$  and  $z$  denote the in-line and cross-flow directions, respectively.  $E$  and  $I$  are Young’s modulus and the area moment of inertia of the pipe, while  $m$  and  $D_s$  denote the mass per unit length and damping coefficient of the riser.  $f_y$  and  $f_z$  represent the external forces of corresponding directions.

Eqs. (8) and (9) can be discretized by finite difference method and solved numerically. And note that those equations are linear equations and thus large rotations are not considered. This pipe motion solver has been validated multiple times by Huang *et al.* (2007, 2010, 2012, 2013).

### 2.4 Fluid-structure interaction procedure

The FSI method adopted in this research is the partitioned approach, in which the existing fluid domain solver, FANS, can be fully utilized by coupling with the riser motion solver presented above. The basic idea of partitioned FSI approach in this paper is illustrated in Fig. 2.

## 3. Results and discussions

### 3.1 Computational grids

A complete cross-section view and an overview of the grid system used in this paper are shown in Figs. 3(a) and 3(b). Two computational blocks are constructed for the VIV simulations including

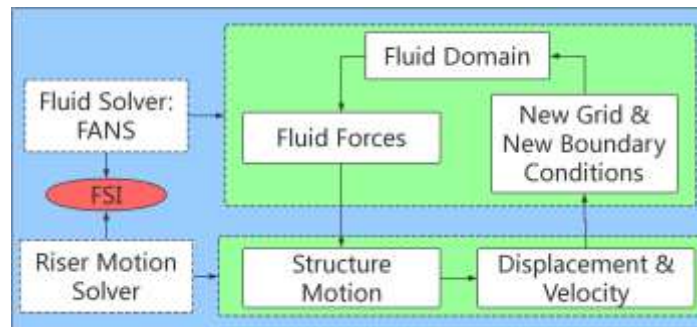
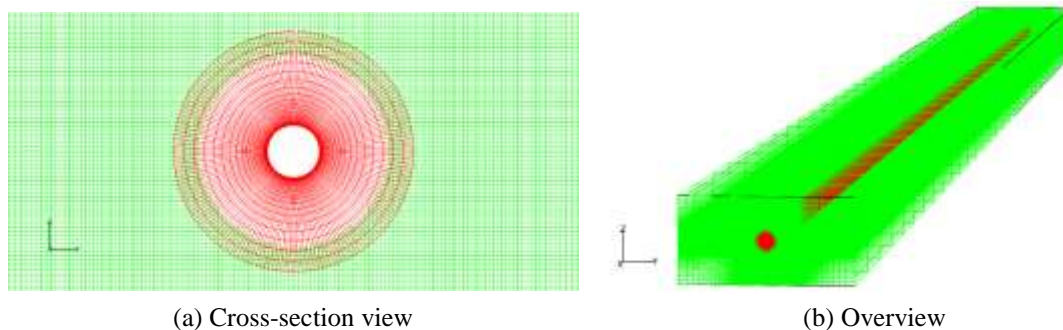


Fig. 2 FSI procedure

the near field block (red) and the background grid block (green). The near field block has 231322 computational points in total with the dimension of 31(axial direction) $\times$ 182(circumferential direction) $\times$ 41(radial direction). The near-wall grid spacing of the near field block is 0.0001 riser diameter. The background block has 629331 grid points in total with the dimension of 31 $\times$ 201 $\times$ 101. The time step size used in this paper is 0.01s. Under these settings, we are able to complete each simulation using a single core with 3.6 GB memory within 36 hours on super clusters in Texas A&M University.

### 3.2 Validation of soil-structure interaction model

To validate the SSI model used in this research, the simplified p-y curve introduced previously is verified in a static load case by comparing the obtained result from the motion solver with the published analytical and Finite Element Analysis (FEA) solutions (Choi and Basu 2013). The case is illustrated in Fig. 4. A riser with a total length of 15m is discretized to 250 segments with a mesh size ( $\Delta x$ ) of 0.06 m is used for this case. A lateral load of 300 kN is applied to the first node of the riser. Soil springs are added to every node of the pipe inside soil to model the later soil resistance force, and both ends of the riser are set free.



(a) Cross-section view

(b) Overview

Fig. 3 Computational Grids

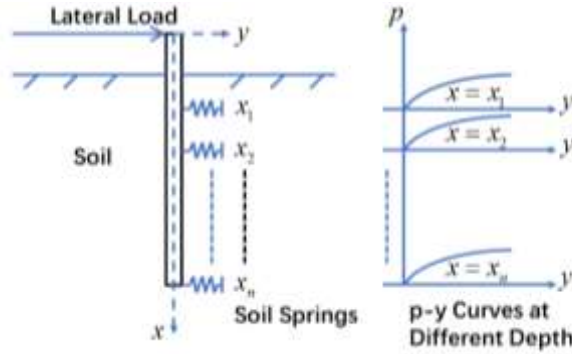


Fig. 4 Case illustration

Table 1 Parameters for validation

Parameter	Units	Value
Pipe Diameter, $d$	$m$	0.6
Soil Shear Strength, $c$	$kPa$	36
Soil Effective Unit Weight, $\gamma$	$N/m^3$	20000
Strain of Half Maximum Stress, $\epsilon_c$	1	0.01
Empirical Constant, $J$	1	0.5

The p-y curves which characterize the soil resistance force are calculated by Eqs. (1)-(3), and (7). It is worth mentioning that the soil lateral ultimate resistance,  $p_u$ , is linearly increasing with soil depth until the soil depth reaches the depth of reduced resistance,  $x_r$ , which in this case is 4.32 m. Therefore, soil resistance is of its lowest value at the free-soil surface, the #1 computation node, and increasing to its maximum value at depth of reduced resistance, the #73 computation node. The parameters used in this case are according to the case published by Choi and Basu (2013) as listed in Table 1.

Results obtained from the riser motion solver used in this research are compared with the results obtained by Choi and Basu (2013), as shown in Fig. 5(a). A good agreement of riser lateral displacement is shown between the present solution and published solutions: the key feature of a negative displacement of the pipe between approximately soil depth of 3m to 8m is captured. The difference between results calculated by the motion solver and the published analytic solution is less than 15%. Therefore, the efficiency of the Soil-Structure Interaction model, as well as the motion solver, is validated. A grid refinement study is conducted to ensure that the result presented above is accurate, which means that the increase in the number of computation points does not change the resolution of the result significantly. As shown in Fig. 5(b), when 125 or more computation points are used, the results are not significantly different. Thus, the use of 250 points with the element length of 0.06 m is nearly grid-independent for computation.

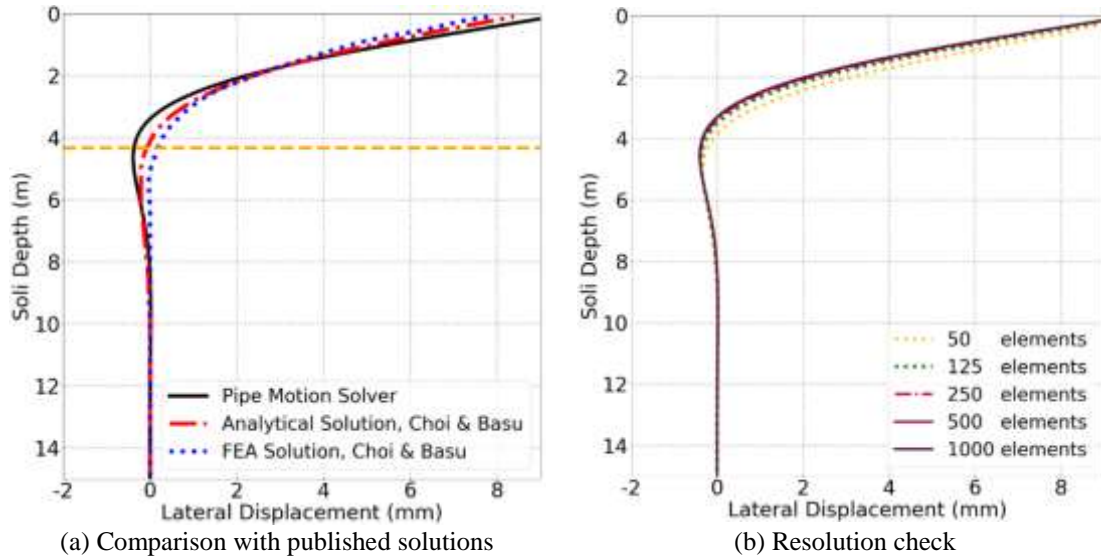


Fig. 5 Validation of SSI model

### 3.3 Benchmark case: VIV simulation of a riser without SSI

In order to systematically study the VIV responses of riser-conductor systems with the soil-structure interactions (SSI), a VIV simulation of a riser without SSI is firstly analyzed, which will also serve as a benchmark case for this research. In this simulation, a full-scale riser is used in this paper with a length-to-diameter ratio ( $L/D$ ) of 482.5 is used in order to get full-scale soil resistance force. The riser vertically stands in the fluid field, and both ends of the riser are pinned. A linearly distributed tension is used since the riser is vertically standing in the fluid. The riser parameters are listed as follows in Table 2. Note that in this paper the BOP is not specifically treated, but more detailed and realistic modeling of the system will be conducted in the future.

Table 2 Riser parameters

Parameter	Units	Value
Riser Diameter	$m$	0.3
Riser Length	$m$	144.45
Bending Stiffness	$N \cdot m^2$	6.85E6
Top Pretension	$N$	1.84E5
Bottom Pretension	$N$	1.75E5

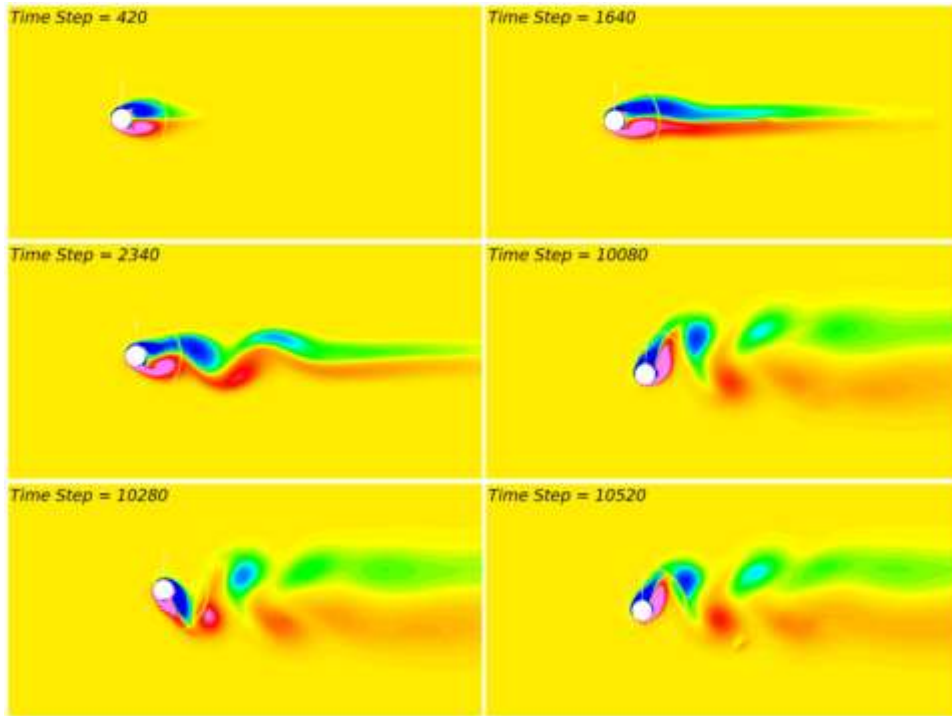


Fig. 6 Vortex generating and shedding, benchmark case

A uniform current of 0.42 m/s is specified for this simulation. Vortex generation process is observed in the early stage. And then the generated vortex starts to detach from the riser surface and cause the riser to oscillate in the cross-flow direction. After time step 5000, vortex generates and detaches from the riser surface regularly under certain frequencies. The fluid field is shown in Fig. 6. For a better understanding of the complete fluid domain, selected cross-sections of a specific time step are provided in Fig. 7.

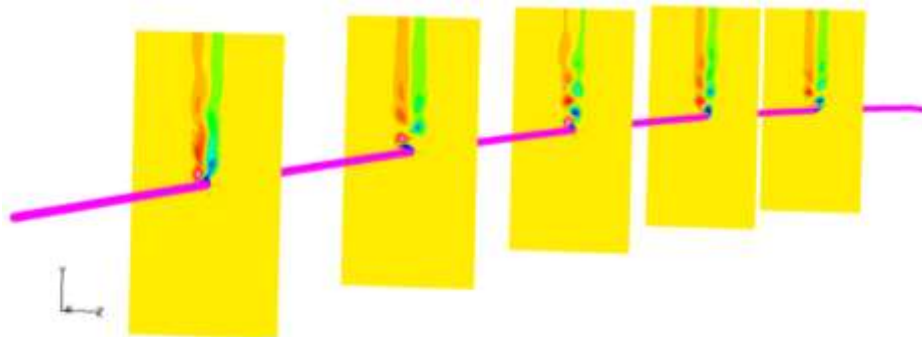


Fig. 7 Fluid filed view, benchmark case

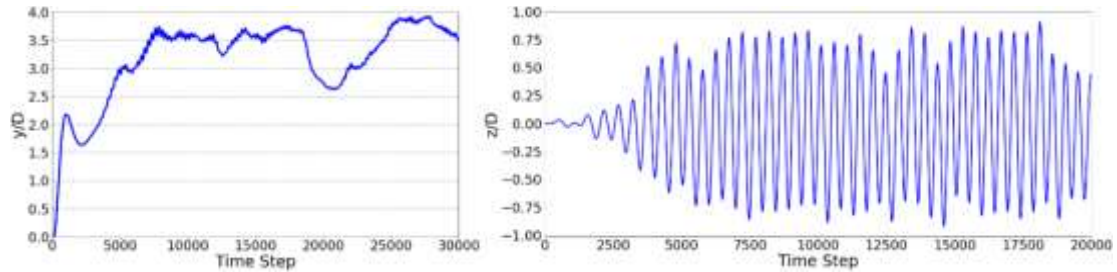


Fig. 8 In-line (left) and cross-flow (right) histories of selected cross sections, benchmark case

Riser motion history for a riser middle cross-section in in-line (left) and cross-flow (right) directions are presented in Fig. 8. Note that the displacement is normalized by the riser diameter, 0.3 m. As shown in the figure, the riser starts to deflect quickly at the beginning of the simulation, then the in-line displacement reduces to about 1.5 riser diameter due to the bending stiffness of the riser itself. The maximum value of the riser in-line deflection is approximately 4.0 times of riser diameter.

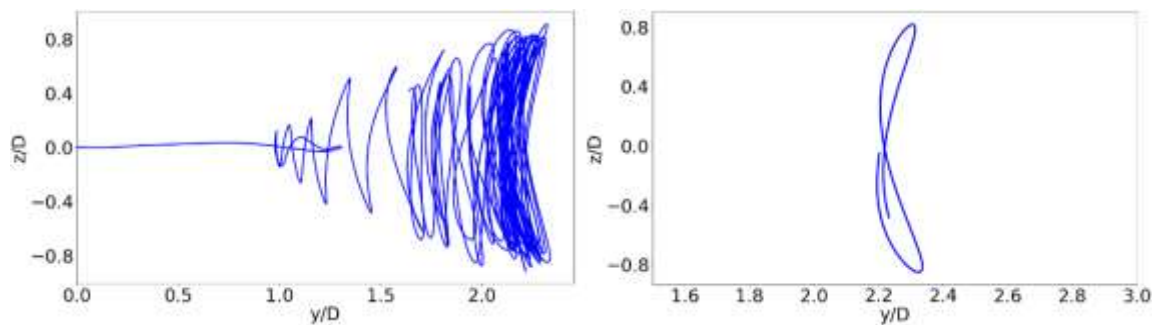


Fig. 9 Riser trajectory, benchmark case

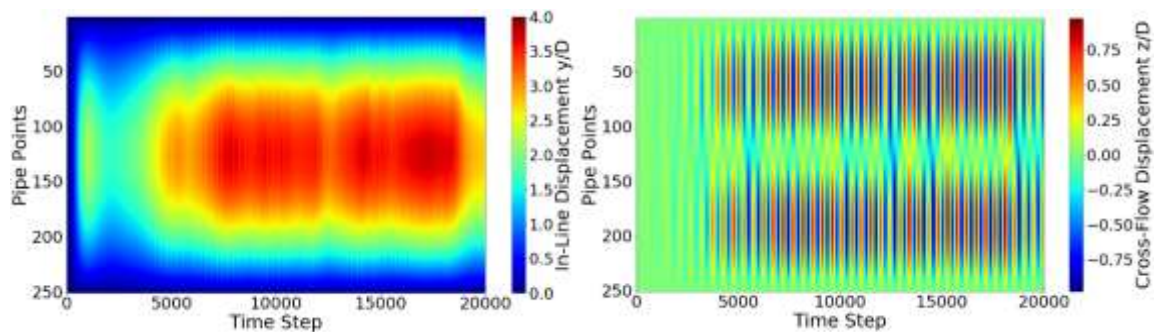


Fig. 10 In-line (left) and cross-flow (right) motion histories, benchmark case

For the cross-flow direction, no significant deflection is shown until time step 2500. Large amplitude vibration with maximum displacement of about 0.8 riser diameters is shown after time step 5000, which is also known as vortex-induced vibrations (VIV).

Fig. 9 shows the trajectory of the riser at the mid-depth in the time step range of 17000 and 17520. A clear riser VIV response pattern deformed “8” is also captured and presented in that figure. The in-line (left) and cross-flow (right) displacement histories for the entire riser are provided in Fig. 10.

### 3.4 VIV simulation of a riser including soil-structure interactions

#### 3.4.1 VIV simulation of a riser with simplified SSI model

The simplified SSI model described by Eq. (7) is first utilized. It is a “partial non-linear” SSI model, for the reason that the soil ultimate resistance,  $p_u$ , is nonlinear in “x” direction, while the p-y relation for each x value is simplified to linear. Soil resistance force is applied to the riser-conductor system in a partitioned coupling method. The soil properties are given in Table 3. It is worth noting that in this case, the depth of reduced resistance,  $x_r$ , calculated by Eq. (3), is 2.7 m, which is 9 times the riser diameter.

The riser in the fluid domain is the same as the benchmark case with a length of 144.45 m and diameter of 0.3 m. An additional half of the total riser length, 72.3 m, is set to be under the soil bed. The riser-conductor system is still pinned at the top whereas setting free at the bottom. The same element length of the riser-conductor system is used in the riser motion solver.

The simulation result in the fluid domain is very similar to the benchmark case. Riser motions are compared with the results from the benchmark case in Fig. 11. In the in-line direction, the riser response is similar to the benchmark case while an up to 40% reduction in in-line deflection is observed. For the cross-flow direction, a similar conclusion can be obtained and a maximum of 30% reduction in magnitude is shown when comparing with the benchmark case.

Comparisons of riser trajectories and spectrums for normalized CF displacements are presented in Fig. 12. As shown in that figure, both in-line and cross-flow displacements are reduced remarkably when SSI is considered. An overview of the whole riser motion history is again provided in Fig. 13.

It should be remarked that the riser-conductor system is not held stationary below the mudline, but the riser vibration amplitude is rather small at the mudline due to the soil resistance of the seabed. As shown in Fig. 14, a maximum magnitude of 0.03 riser diameter in in-line direction and 0.02 riser diameter in cross-flow direction is observed.

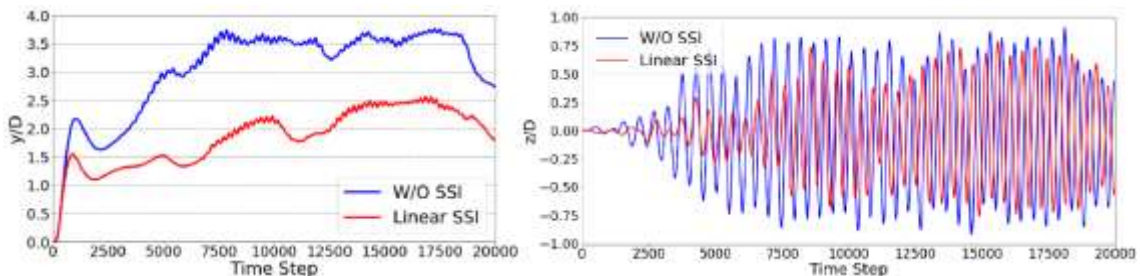


Fig. 11 Comparison of in-line (left) and cross-flow (right) motions

Table 3 Soil properties, 1

Parameter	Units	Value
Soil Shear Strength, $c$	kPa	36
Soil Effective Unit Weight, $\gamma$	$N/m^3$	20000
Strain of Half Maximum Stress, $\epsilon_c$	1	0.009
Empirical Constant, $J$	1	0.5

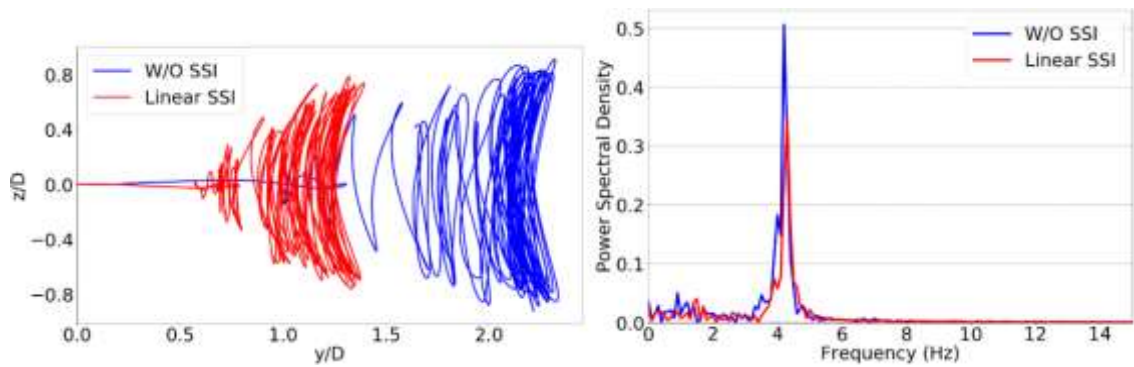


Fig. 12 Comparison of riser trajectories (left) and cross-flow responses

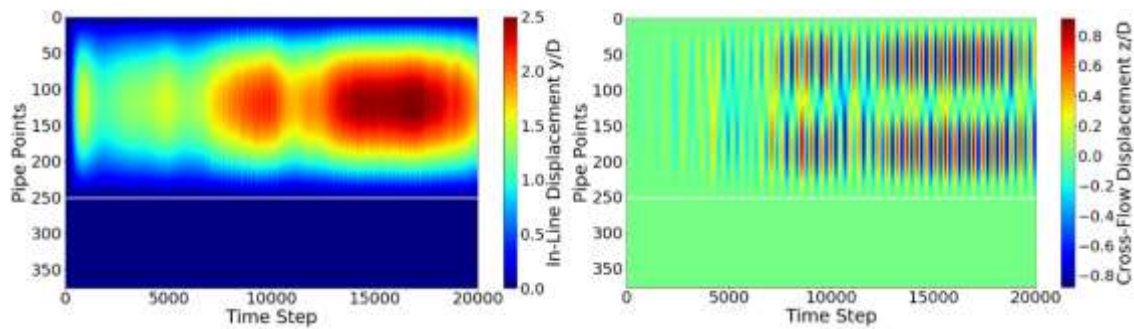


Fig. 13 In-line (left) and cross-flow (right) motion histories, simplified SSI

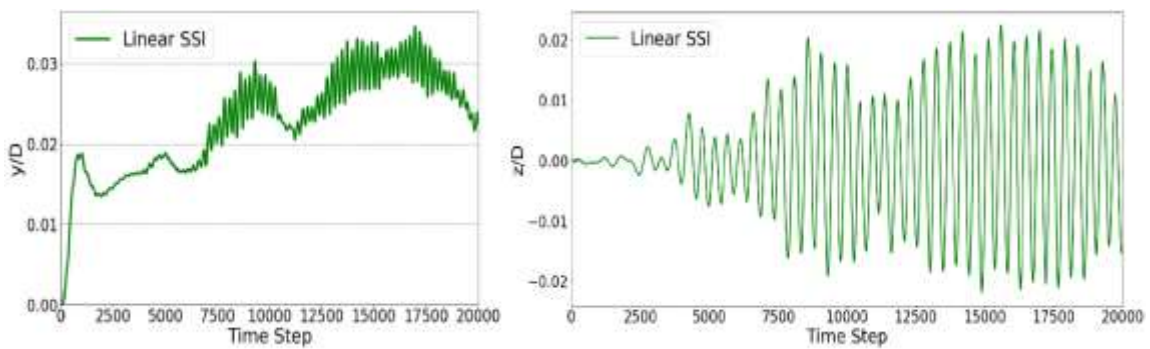


Fig. 14 In-line (left) and cross-flow (right) motion at mudline, simplified SSI

Table 4 Soil properties, nonlinear SSI

Parameter	Units	Value
Riser-conductor system Diameter	m	0.3
Riser-conductor system length in Fluid Domain	m	144.45
Riser-conductor system length in Soil	m	72.23
Bending Stiffness	$N \cdot m^3$	6.85E6
Top Pretension	m	1.84E5
Soil Shear Strength, $c$	kPa	36
Soil Effective Unit Weight, $\gamma$	$N/m^3$	20000
Strain of Half Maximum Stress, $\epsilon_c$	1	0.009
Empirical Constant, $J$	1	0.5
Depth of Reduced Resistance, $x_r$	m	2.7

3.4.2 VIV simulation of a riser with nonlinear SSI model

The fully nonlinear SSI model illustrated in Eq. (5) is then applied to VIV simulations. Soil properties and riser-conductor system parameters are the same as the last case, as listed in Table 4.

The fluid domain view at  $x/L=0.4$  for this case is similar to the previous two cases, as shown in Fig. 15. And as shown in Figs. 16 and 17, riser motions in the fluid domain obtained by the two different SSI models are similar.

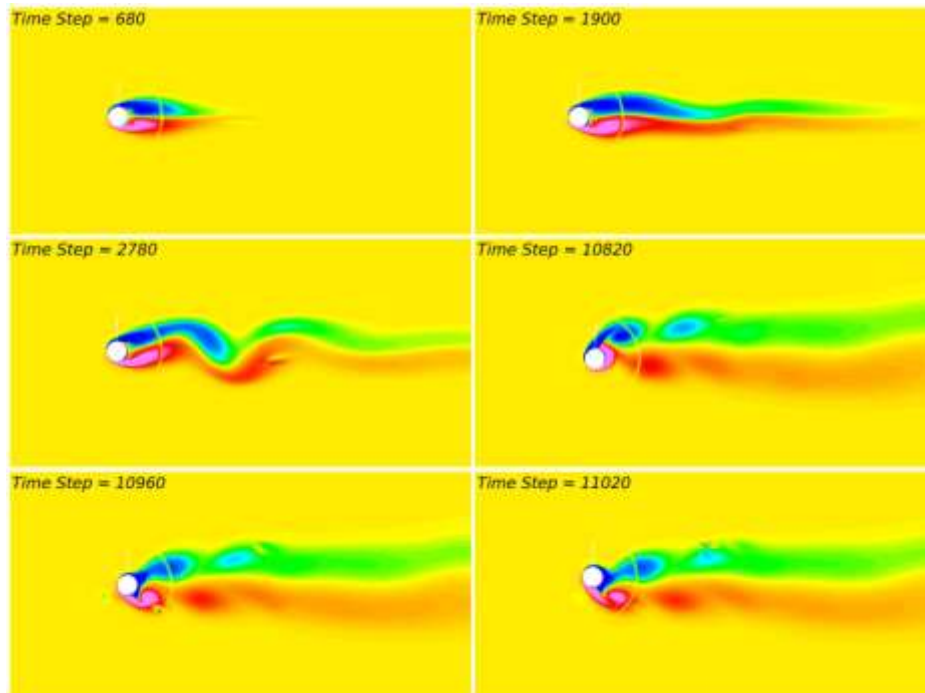


Fig. 15 Vortex generating and shedding, nonlinear SSI

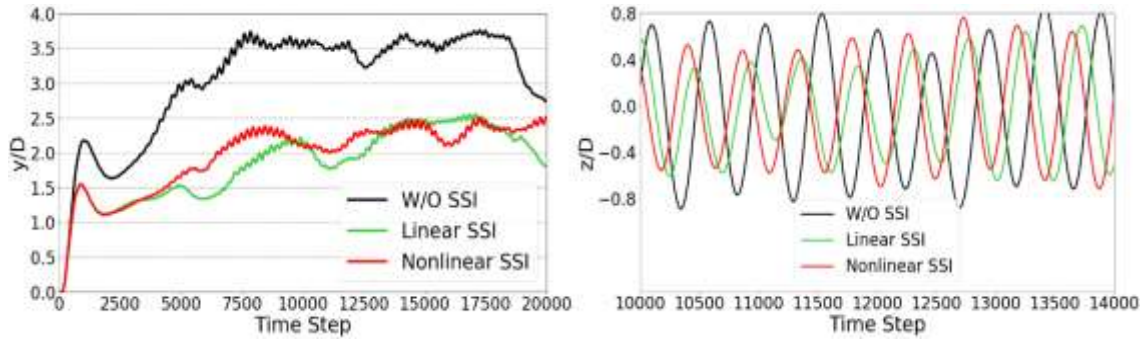


Fig. 16 Comparison of in-line (left) and cross-flow (right) motions, nonlinear SSI

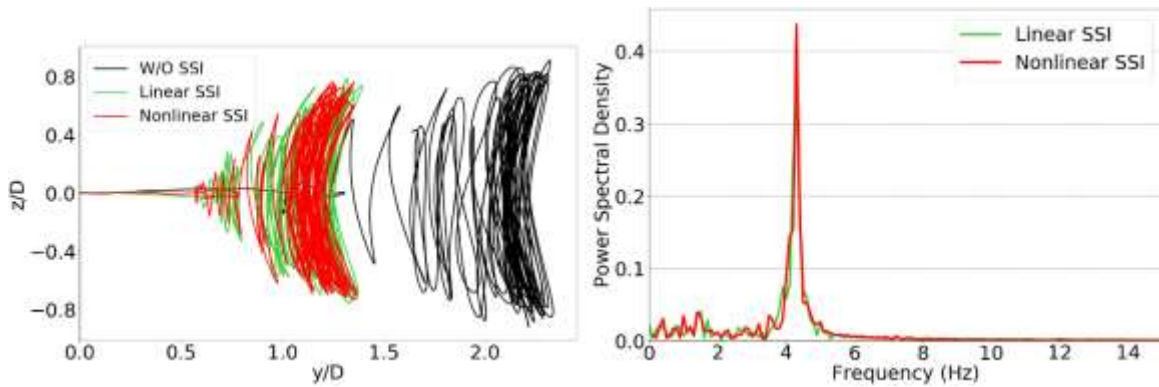


Fig. 17 Comparison of riser trajectories (left) and cross-flow responses, nonlinear SSI

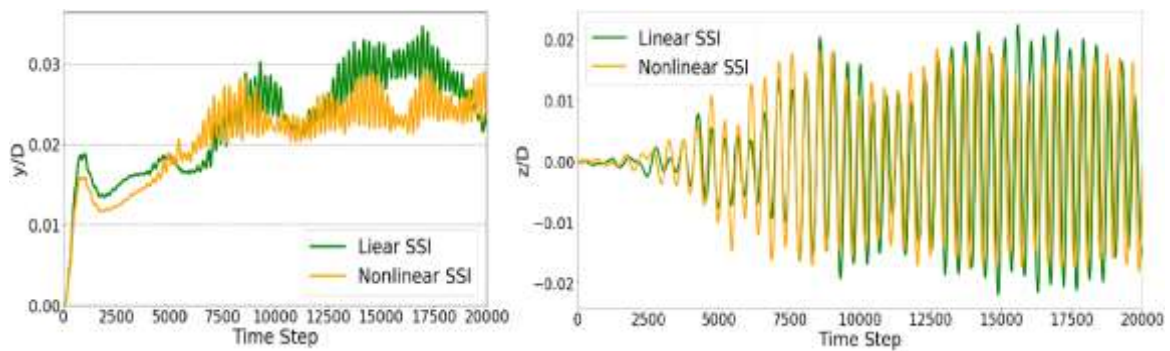


Fig. 18 Comparison of in-line (left) and cross-flow (right) motions at mudline

Riser-conductor system motions at mudline are compared in Figs. 18 and 19. As shown in riser in-line and cross-line motions, a considerable difference of magnitude is observed. Comparing to the simplified SSI model, result from nonlinear SSI model is smaller. For both cases, the lateral

displacements are smaller than  $y_c$ , therefore, the simplified linear SSI model will apply a smaller soil resistance force to the riser-conductor system comparing to the nonlinear model described by Eq. (5), which means smaller displacement will be obtained from the nonlinear SSI model. For completeness, a direct comparison of the riser trajectories for the linear and nonlinear SSI models are provided in Fig. 19, in which we can clearly see that the trajectory from nonlinear SSI model is confined to a smaller area as discussed above. The motion envelopes of the system in in-line and cross-flow directions near mudline are shown in Fig. 20. As we can see, while the envelopes of two SSI models are similar, a remarkable difference comparing to the benchmark case is observed due to the presence of soil resistance force.

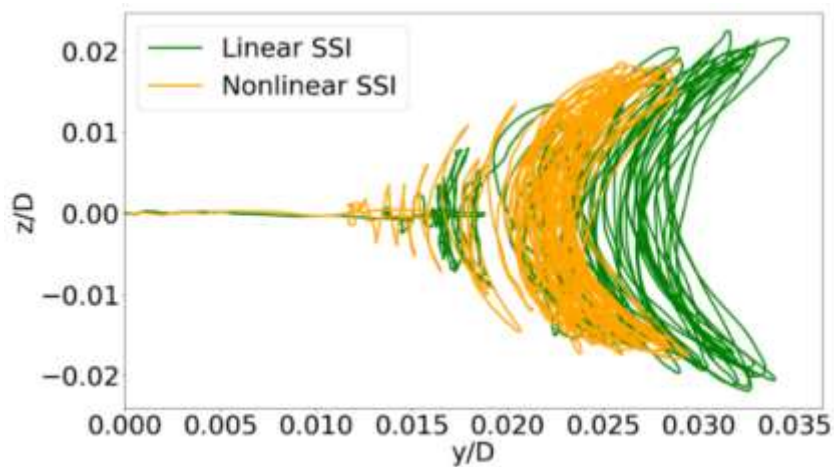


Fig. 19 Trajectories at mudline

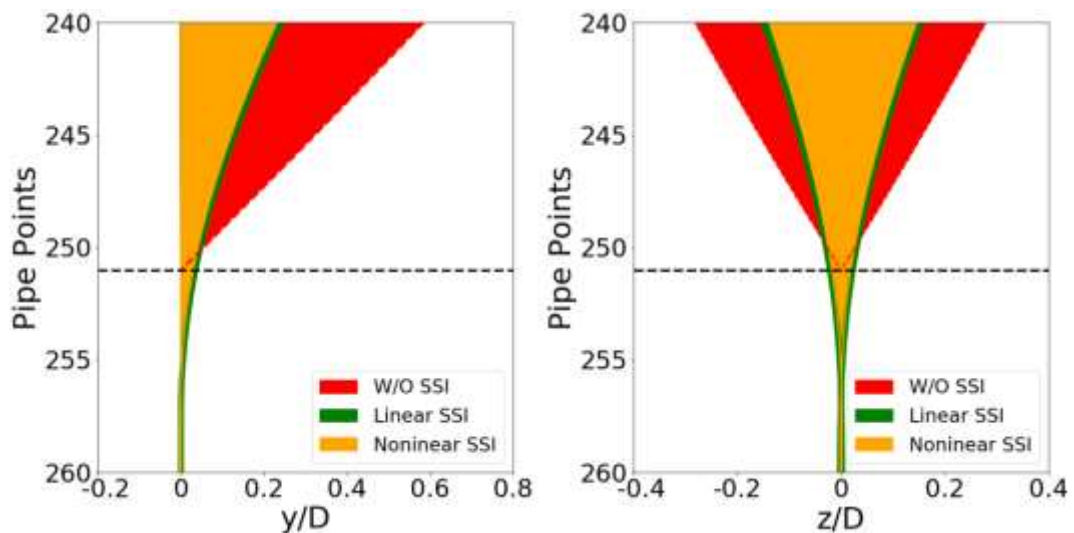


Fig. 20 Comparison of in-line (left) and cross-flow (right) motion envelopes near mudline

### 3.5 Effects of soil properties on riser-conductor system VIV simulations

Soil strength  $c$  and soil effective unit weight  $\gamma$  are two key parameters that characterize soil properties, thus further clarification is required for analysis. In earlier discussions,  $c$  and  $\gamma$  were arbitrarily set to 36 kPa and  $20000 \text{ N/m}^3$ , respectively, according to the commonly used values. In this section, the effects of the two aforementioned soil properties on the VIV simulations are studied. Note that the nonlinear SSI model is selected in the following simulations. First, riser-conductor system VIV simulation with soil strength of 12 kPa, 24 kPa and 36 kPa are performed, with a same soil effective weight of  $20000 \text{ N/m}^3$ . Motion histories at mudline are given in Fig. 21. As shown in Fig. 22, the trajectory from  $c = 36 \text{ kPa}$  is on the left, while the trajectory from  $c = 12 \text{ kPa}$  is on the right. It can be concluded that with decreasing soil strength, riser motion magnitude increases. That is reasonable since larger soil strength results in larger soil resistance force which confines the riser-conductor system trajectory to a smaller area. The maximum displacement in in-line and cross-flow directions obtained from those three cases are also compared in Fig. 22. Apparently, the maximum displacement reduces with the increasing soil shear strength.

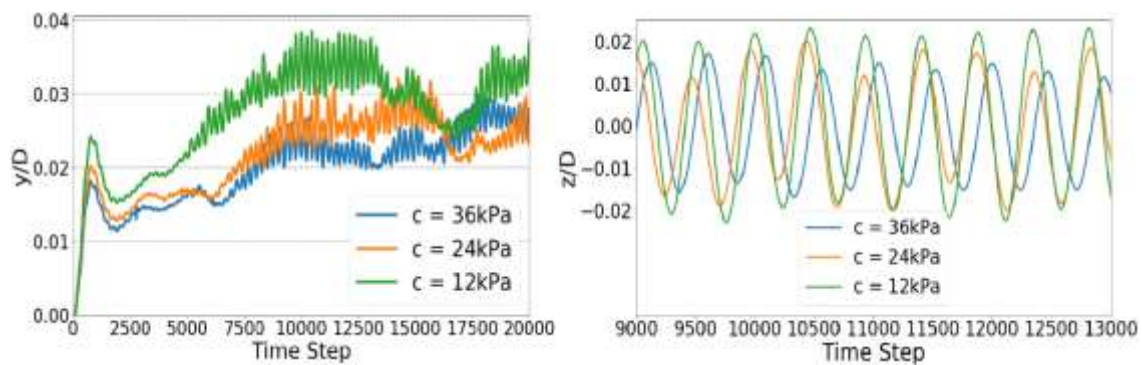


Fig. 21 In-line (left) and cross-flow (right) motions at mudline for different soil strength

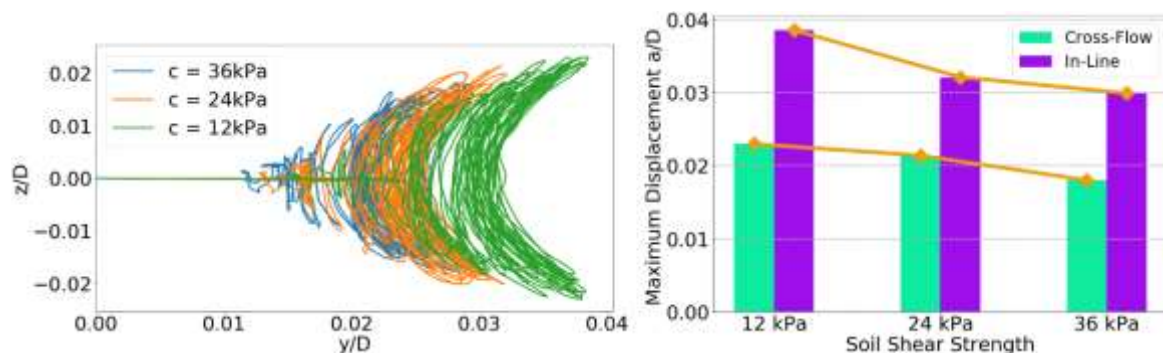


Fig. 22 Trajectories (left) and maximum displacements (right) for different soil strength at mudline

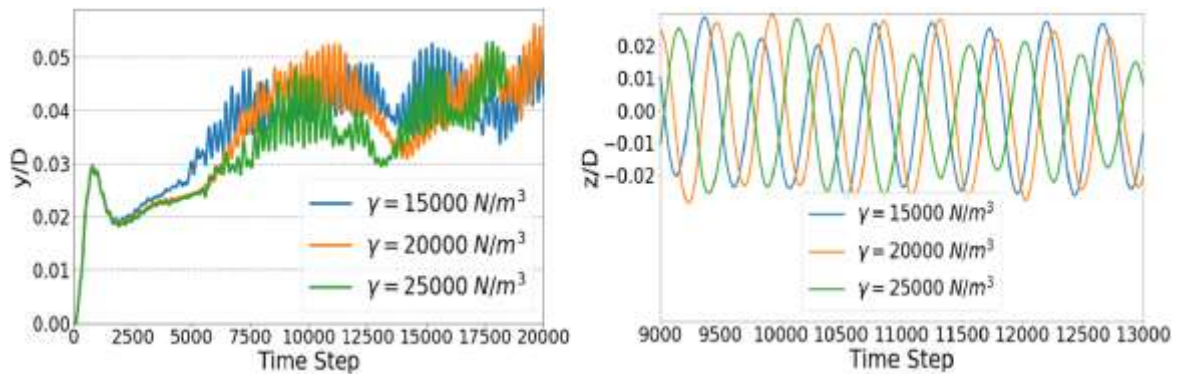


Fig. 23 In-line (left) and cross-flow (right) motions at mudline for different soil unit weight

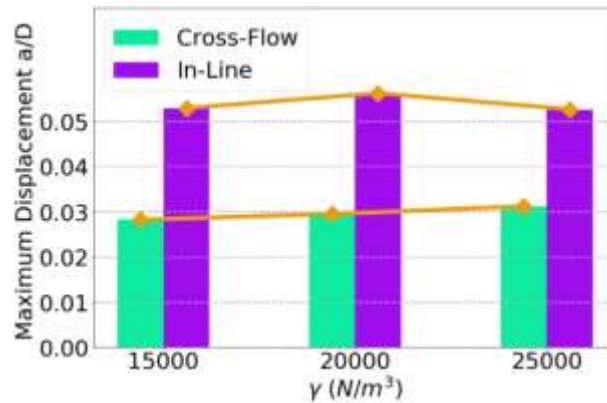


Fig. 24 In-line (left) and cross-flow (right) motions at mudline for different soil unit weight

Three different soil effective unit weight,  $15000 N/m^3$ ,  $20000 N/m^3$  and  $25000 N/m^3$  with the same value of soil strength, are then applied to the VIV simulations. Riser-conductor system motions are shown in Fig. 23. The maximum displacements in in-line and cross-flow directions with varying  $\gamma$  are also provided in Fig. 24. No significant change in magnitude is observed when soil effective unit weight increases.

#### 4. Conclusions

Deepwater drilling riser-conductor systems are susceptible to VIV. Previous researchers have rarely taken soil-structure interactions (SSI) into account when discussing the VIV response of riser-conductor systems, and experimental data of riser-conductor system VIV including SSI is especially absent. In this paper, a numerical approach for riser-conductor VIV analysis is developed by coupling the fluid domain solver, Finite-Analytic Navier-Stokes (FANS) code, and the riser motion solver including the SSI models. The SSI is reached by modeling the soil

resistance force according to nonlinear p-y curves which specify the relationship between riser-conductor system lateral displacement and soil resistance force.

First, the riser-conductor system is modeled as a distributed tension beam, and the soil model is validated by a case in which static force is applied. Second, a riser VIV simulation without considering SSI is chosen as a benchmark case for the subsequent simulations of soil-structure interactions. A simplified SSI model is then used in the riser-conductor system VIV simulation, and a significant reduction of 20% to 40% in magnitude in both in-line and cross-flow directions are observed. Riser-conductor system motion at mudline is also obtained instead of zero displacement in the benchmark case. Following the simplified SSI model, the fully nonlinear SSI model is applied to the VIV simulation. The result is similar to the simplified SSI model case in magnitude. Finally, the effect of two key soil properties on the riser-conductor system VIV simulations is discussed. It is shown that the vibration amplitude of the system at mudline is amplified when soil shear strength decreases.

In conclusion, a fully three dimensional CFD approach for analyzing the VIV of deepwater drilling and production riser-conductor systems is provided. This research contributes knowledge and insight to future design and analysis of riser-conductor systems.

## References

- Ai, S. and Sun, L. (2010), "Vortex induced vibration response of a rigid cylinder supported with perfectly plastic nonlinear springs", *J. Vib. Shock*, **29**(11), 21-25.
- Basu, D. and Salgado, R. (2007), "Elastic analysis of laterally loaded pile in multi-layered soil", *Geomech. Geoeng.*, **2**(3), 183-196.
- Cao, Y. and Chen, H.C. (2017), "CFD simulation of vortex-induced vibration of free-standing hybrid riser", *Ocean Syst. Eng.*, **7**(3), 195-223.
- Chen, H.C., Chen, C.R. and Huang, K. (2013), "CFD simulation of vortex-induced and wake-induced vibrations of dual vertical risers", *Proceedings of the 23rd (2013) International Offshore and Polar Engineering*, Anchorage, Alaska, USA, July.
- Chen, H.C., Patel, V.C. and Ju, S. (1990), "Solutions of Reynolds-Averaged Navier-Stokes equations for three-dimensional incompressible flows", *J. Comput. Phys.*, **88**(2), 305-336.
- Choi, Y.S., Basu, D., Salgado, R. and Prezzi, M. (2014), "Response of Laterally Loaded Rectangular and Circular Piles in Soils with Properties Varying with Depth", *J. Geotech. Geoenviron. Eng.*, **140**(4), 04013049.
- El Naggar, M.H. and Novak, M. (1995), "Nonlinear lateral interaction in pile dynamics", *Soil Dynam. Earthq. Eng.*, **14**(2), 141-157.
- Gazetas, G. and Dobry, R. (1984), "Horizontal response of piles in layered soils", *J. Geotech. Eng.*, **110**(1), 20-40.
- Han, F., Salgado, R. and Prezzi, M. (2015), "Nonlinear analyses of laterally loaded piles – a semi-analytical approach", *Comput. Geotech.*, **70**, 116-129.
- Huang, K., Chen, H.C. and Chen, C.R. (2007), "Riser VIV analysis by a CFD approach", *Proceedings of the 17<sup>th</sup> International Offshore and Polar Engineering (ISOPE) Conference*, Lisbon, July.
- Huang, K., Chen, H.C. and Chen, C.R. (2010), "Vertical riser viv simulation in uniform current", *J. Offshore Mech. Arctic Eng.*, **132**(3), 395-405.
- Huang, K., Chen, H.C. and Chen, C.R. (2011), "Numerical scheme for riser motion calculation during 3-D VIV simulation", *J. Fluid. Struct.*, **27**(7), 947-961.
- Huang, K., Chen, H.C. and Chen, C.R. (2012), "Vertical riser viv simulation in sheared current", *Int. J. Offshore Polar Eng.*, **22**(2), 142-149.

- Ilupeju, O.A. (2014), "Soil-spring model for fatigue evaluation of cyclic-loaded offshore conductors", Master of Science Thesis; Texas A&M University, College Station, Texas, USA.
- Kamble, C. and Chen, H.C. (2016), "CFD prediction of vortex induced vibrations and fatigue assessment for deepwater marine risers", *Ocean Syst. Eng.*, **6**(4), 325-344.
- Liang, A., Wang, S., Li, L., Liu, X., Wang, Z. and Wen, X. (2014), "Study on influence of soil-pile nonlinear interaction on vehicle-bridge coupling vibration", *Eng. Mech.*, **31**(12), 96-103.
- Matlock, H. (1970), "Correlation for design of laterally loaded piles in soft clay", *Offshore Technol. Civil Eng.*, **1**, 77-94.
- Matlock, H. and Reese, L.C. (1960), "Generalized solutions for laterally loaded piles", *Geotechnical Special Publication*, **127**(118), 1220-1248.
- Nogami, T. and Konagai, K. (1988), "Time domain flexural response of dynamically loaded single piles", *J. Eng. Mech.*, **114**(9), 1512-1525.
- Nogami, T., Konagai, K. and Otani, J. (1991), "Nonlinear time domain numerical model for pile group under transient dynamic forces", *International Conferences on Recent Advances in Geotechnical Earthquake Engineering and Soil Dynamics*, 25.
- Novak, M. and Works, V.I. (1974), "Dynamic stiffness and damping of piles", *Can. Geotech. J.*, **11**(4), 574-598.
- Pontaza, J.P. and Menon, R.G. (2009), "Prediction of VIV response of a flexible pipe by coupling a viscous flow solver and a beam finite element solver", *Proceedings of the 28th Intl Conference on Ocean, Offshore and Arctic Engineering*, Honolulu, Hawaii, USA, June.
- Pontaza, J.P., Chen, C.R. and Chen, H.C. (2004), "Chimera reynolds averaged Navier-Stokes simulations of vortex-induced vibration of circular cylinders", *Proceedings of the International ASCE Conference: Civil Engineering in the Oceans VI*.
- Reese, L.C. (1974), "Analysis of laterally loaded piles in sand", *Offshore Technical Conference*, 95-105.
- RP 2A-WSD (2010), Recommended Practice for Planning, Designing and constructing fixed offshore platforms—working stress design, American Petroleum Institute; Washington, D.C., USA.
- Tognarelli, M.A., Taggart, S. and Campbell, M. (2008), "Actual VIV fatigue response of full scale drilling risers: with and without suppression devices", *Proceedings of the ASME 2008 27th International Conference on Offshore Mechanics and Arctic Engineering*.
- Trim, A.D., Braaten, H., Lie, H. and Tognarelli, M.A. (2005), "Experimental investigation of vortex-induced vibration of long marine risers", *J. Fluid. Struct.*, **21**, 335-361.
- Wilde J.J. and Huijsmans, R.H. (2004), "Laboratory investigation of long riser VIV response", *Proceedings of the 14th International Offshore and Polar Engineering Conference*, Toulon, France, May.
- Xiao, F. (2015), "CFD simulation of vortex-induced vibrations of free span pipelines including pipe-soil interactions", *Proceedings of the 25th International Offshore and Polar Engineering Conference*, Kona, Hawaii, USA, June.
- Yao, W., Huai-Rui, W., Cheng, Z. and Wu, Y. (2011), "Nonlinear numerical analysis of super-long piles based on p-y curves", *Chinese J. Geotech. Eng.*, **33**(11), 1683-1690.
- Zhu, Y. (2017), "Numerical simulation of vortex-induced vibrations of free span pipelines including nonlinear soil models", Master of Science Thesis; Texas A&M University, College Station, Texas, USA.